Soils and Rocks
An International Journal of Geotechnical and Geoenvironmental Engineering
www.soilsandrocks.com
ISSN 1980-9743
ISSN-e 2675-5475

Undrained monotonic behavior of a dune sand stabilized with porcelain waste and lime

José Daniel Jales Silva[1#], Olavo Francisco dos Santos Júnior[2], Osvaldo de Freitas Neto[2], Romário Stéffano Amaro da Silva[2], Manoel Leandro Araújo e Farias[1], Bruna Silveira Lira[1]

Article

Keywords
Triaxial test
Soil liquefaction
Soil stabilization
Industrial wastes

Abstract

This work uses a new cementitious agent composed of porcelain polishing waste and hydrated lime in the mitigation of static liquefaction in a loose dune sand. The undrained behavior of the soil was investigated in 16 triaxial tests under four confining stresses (50, 100, 200 and 400 kPa), on loose samples (relative density of 25%) compacted with two levels of waste (10% and 30%) and lime contents (3% and 7%) cured at 28 days. Stress-strain behavior, ultimate strength and critical state parameters were evaluated. The results showed a brittle response of the stabilized sands, dilatant tendency and low liquefaction potential, however, the behavior changes with the increase in the confining stress. A friction angle of up to 42.6° and a cohesion intercept of up to 108.1 kPa were found for the stabilized sand. When compared to the pure sand, stabilization caused an increase in strength, of up to 17 times, and in brittleness with a change from contractive to dilatant behavior. For tests up to 200 kPa, the liquefaction potential reduced to values below zero. Therefore, the cementation of the grains by using porcelain polishing waste and hydrated lime was efficient in mitigating the static liquefaction potential of the dune sand.

1. Introduction

When subjected to monotonic or cyclic loading under undrained conditions, saturated sandy soils in loose state, due to a contractive tendency, can develop large excess pore pressure, which reduces the acting effective stresses and cause a sudden loss of strength, stiffness and bearing capacity, characterizing the liquefaction phenomenon (Castro & Poulos, 1977; Ishihara et al., 1975). As a result, large deformations occur that generate substantial loads on buildings and the entire local infrastructure, which can cause collapses and numerous losses of human lives (Gautam et al., 2017).

In the last decades, research has been carried out in order to understand the mechanisms and factors associated with the triggering of liquefaction (Ghadr & Assadi-Langroudi, 2019; Mahmoudi et al., 2020; Ni et al., 2022; Triantafyllos et al., 2020; Yang et al., 2022; Zhu et al., 2021), assess the susceptibility of natural or artificial deposits to this phenomenon and map the risk in areas of great social interest (Fergany & Omar, 2017; Gautam et al., 2017; Sana & Nath, 2016), in addition to developing techniques that can reduce their probability of occurrence or mitigate their effects on structures (Minyong et al., 2022; Riveros & Sadrekarimi, 2020; Xiao et al., 2019).

As an alternative to the use of traditional liquefaction mitigation techniques, most recent studies investigate new methods such as passive remediation (Krishnan & Shukla, 2021), microbial geotechnologies (Sharma et al., 2021) and the use of fibers (Zhang & Russell, 2021), nanomaterials (Zhao et al., 2019) or biopolymers (Smitha & Rangaswamy, 2021). Although these methods are efficient, some challenges and limitations are encountered in the application over large areas in the field, such as the possibility of non-uniform transmission of the stabilizer, improper monitoring and control of biochemical reactions and the formation of undesirable products that cause impacts on the environment. In addition, they are not easily accessible materials and can have high production and application costs depending on the region.

On the other hand, the need to adopt increasingly sustainable geotechnologies has led to the use of industrial by-products in stabilization operations, as a way of reducing the problems associated with their disposal and production costs. Wastes such as fly ash (Horpibulsuk et al., 2009; Mahvash et al., 2018; Simatupang et al., 2020), glass

#Corresponding author. E-mail address: josedanieljales@gmail.com
[1]Universidade Federal de Campina Grande, Unidade Acadêmica de Engenharia Civil, Campina Grande, PB, Brasil.
[2]Universidade Federal do Rio Grande do Norte, Departamento de Engenharia Civil, Natal, RN, Brasil.

Submitted on November 9, 2023; Final Acceptance on October 10, 2024; Discussion open until May 31, 2025.
Editor: Renato P. Cunha
https://doi.org/10.28927/SR.2025.011023

powder (Baldovino et al., 2020; Consoli et al., 2019a, 2021) and biomass ash (Consoli et al., 2019b; Ghorbani et al., 2018) can be effectively incorporated into mixtures and has been used to improve the performance of geotechnical constructions. However, little research has been conducted on mitigating liquefaction potential of soils with the use of these materials (Keramatikerman et al., 2017; Kolay et al., 2019; Wang et al., 2021).

In this context, porcelain polishing waste (PPW), a component of great worldwide production (Matos et al., 2018b), can also be used. This waste, usually discarded in landfills, requires large storage areas in industries and because of its high fineness, can be a source of soil and groundwater contamination, or even be carried by the winds, affecting the local vegetation. Originating from the operation of polishing porcelain tiles with abrasive materials, it has high pozzolanic activity (Jacoby & Pelisser, 2015; Matos et al., 2018a) and has already been used in the production of ceramics, cements, mortars and concretes (Li et al., 2021; Matos et al., 2020; Medeiros et al., 2021; Sousa et al., 2022), providing significant gains in the mechanical properties and durability of these composites.

Silva et al. (2023) obtained an increase in the compressive and tensile strength of an aeolian sand improved by incorporating PPW and hydrated lime, which was directly proportional to the cementing agent content and curing time. The alkaline activation of PPW can generate cementitious compounds through pozzolanic reactions that act in the creation of a more solid and resistant structure. However, no research was found that evaluated the use of this composite to reduce the liquefaction potential of susceptible soils, thus constituting the main gap that this study aims to address.

Therefore, the aim of this work was to investigate the stabilization of a loose, saturated dune sand subjected to static loading in the undrained condition by adding a new stabilizer composed of porcelain polishing waste and hydrated lime, checking whether this material can improve mechanical performance and reduce the static liquefaction potential of the soil. Souza Júnior et al. (2020) have already confirmed the high liquefaction potential of Natal sand, soil used in this study. The paper contributes to the understanding of the stress-strain behavior of soils cemented with alternative materials to traditional agents such as Portland cement. It also allows evaluating the influence of this stabilizer on the soil strength and critical state parameters.

2. Materials and methods

2.1 Materials

Dune sand, waste from the porcelain tile polishing process and hydrated lime were the three materials used in this research. In Figure 1, the morphology of each material after the preparation process can be visualized, through photography and micrographs obtained by scanning electron microscopy. Figure 2 shows their grain size distribution curves.

The soil is a clean quartz sand of aeolian origin, with angular to subangular particles, collected in a coastal dune in the city of Natal, Brazil. The material was oven dried at 100°C for 24 hours before use. It has a uniform grain size distribution, inserted in the range of fine to medium sand and with a fine content of less than 5%, classified as a poorly graded sand (SP) by the Unified Soil Classification System. The physical properties of the sand are shown in Table 1 and the chemical composition of each material is shown in Table 2.

The porcelain polishing waste was collected in a ceramic industry in the state of Paraíba, Brazil. The PPW was oven dried at 100°C for 24 hours and then manually crushed. It is a fine-grained material, with 26.93% clay (<0.002 mm), 71.61% silt (0.002-0.06 mm) and only 1.46% sand (0.06-0.2 mm). It also has 99.74% of particles smaller than 75µm (Figure 2) and a plasticity index of 4%, classified as a low plasticity silt (ML). The specific gravity found was 2.55 value close to

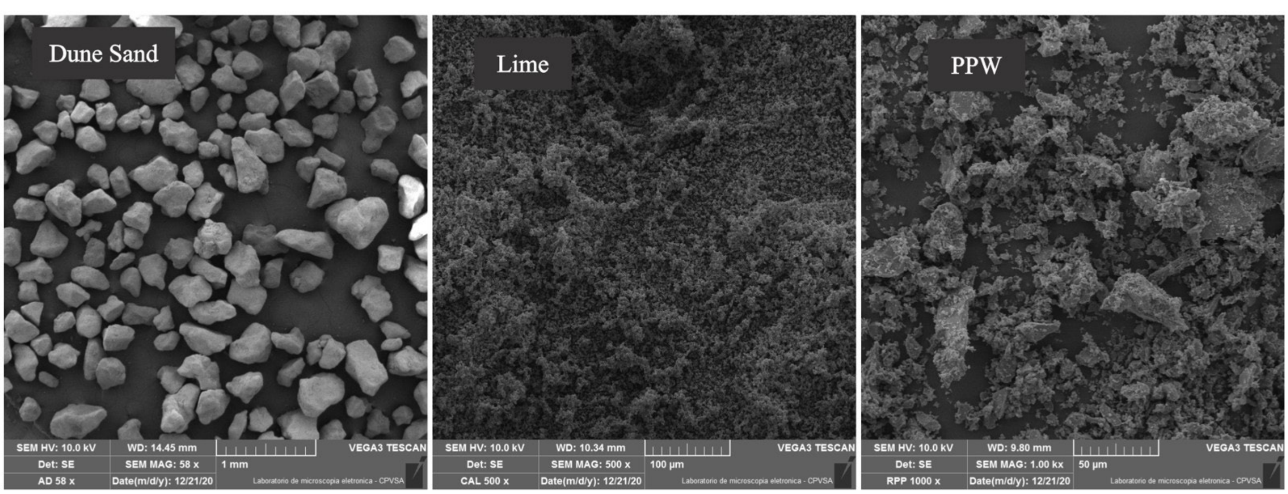

Figure 1. Morphology of dune sand, hydrated lime and PPW.

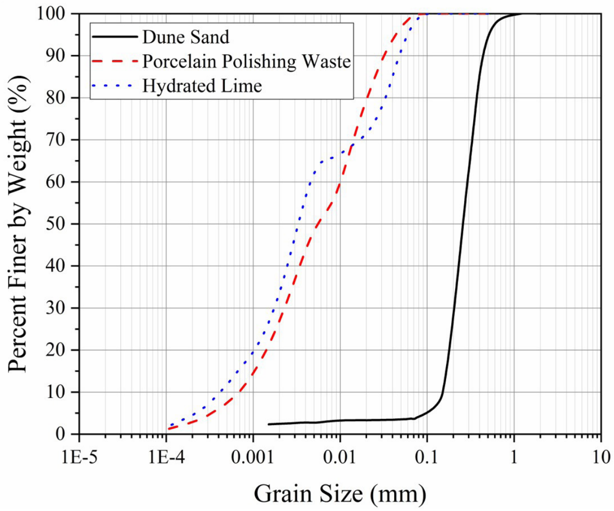

Figure 2. Grain size distribution curves of dune sand, PPW and hydrated lime.

Table 1. Physical properties of dune sand.

Properties	Symbol	Value
Specific gravity	G_s	2.66
Mean diameter (mm)	d_{50}	0.265
Effective diameter (mm)	d_{10}	0.151
Coefficient of uniformity	C_u	1.94
Coefficient of curvature	C_c	0.98
Maximum void ratio	e_{max}	0.84
Minimum void ratio	e_{min}	0.60

Table 2. Chemical composition of dune sand, PPW and hydrated lime.

Compound	Dune sand	PPW	Lime
SiO_2	75.29	67.48	1.88
Al_2O_3	14.57	17.91	0.97
Fe_2O_3	1.97	1.01	0.37
CaO	0.19	3.32	94.07
TiO_2	2.18	0.33	-
MgO	1.6	3.6	0.9
K_2O	1.64	3.55	0.94
NaO_2	1.6	2.0	0.5
SO_3	0.4	0.11	0.11
Others	0.56	0.69	0.26

that found in other studies (Li et al., 2021; Matos et al., 2020; Medeiros et al., 2021). The chemical analysis identified silica and aluminum as the main constituents. Iron, calcium, sodium, magnesium and potassium are present in smaller amounts. As for the mineralogy, quartz, albite, mullite and silicon carbide were identified as the main crystalline phases, the first three probably coming from the porcelain paste and the last one from the abrasive material used in the polishing process. Applying the Modified Chapelle method, a consumption of 394 mg of calcium oxide per gram of PPW was found, confirming its pozzolanic activity. The morphology of PPW is characterized by rough and angular particles of irregular shape. High purity hydrated lime, with a specific gravity of 2.30, was used as the alkaline activator.

2.2 Methods

In this study, the shear strength under undrained conditions of a dune sand stabilized with different contents of porcelain polishing waste (10% and 30%) and hydrated lime (3% and 7%) was evaluated through monotonic triaxial tests in loose compacted samples (relative density of 25%). The lime contents, defined in addition to the mass of sand plus PPW, were chosen based on the minimum content of 3% found by the Initial Lime Consumption method proposed by Rogers et al. (1997) and in accordance with other studies that used pozzolan-lime mixtures for soil improvement (Abbasi & Mahdieh, 2018; Consoli et al., 2019b, 2021).

The PPW contents, defined as a substitute for sand in the mixture, were determined to evaluate the effects of different incorporation contents. Previous tests have shown that levels below 10% are ineffective. Furthermore, the studies with pozzolan-lime mixtures cited above have shown that an increase in pozzolan content tends to amplify pozzolanic reactions, providing gains in soil strength, justifying the high values adopted. The low relative density was chosen due to the high liquefaction potential presented by samples of pure sand in the loose state (Souza Júnior et al., 2020). For each composition, maximum and minimum void ratio tests were performed. Table 3 presents the physical properties of the samples with a Code of sample XPYL where the X represents the amount of PPW and the Y the amount of Lime. This Code was used in all paper.

2.3 Molding and curing of the specimens

The specimens, with dimensions of 50 mm in diameter and 100 mm in height, were prepared using the moist tamping technique, as it allows the obtainment of more homogeneous samples in an extensive range of densities through simple procedures (Sze & Yang, 2014). Furthermore, this method allows a better dispersion of the stabilizer in the sand matrix, avoiding eventual segregation and concentration of grains that could occur in other methods.

Initially, sand and PPW in the dry condition were mixed until a homogeneous appearance was obtained. Then, lime was added and a new mixture was performed. Distilled water was added to the final material. The mass of each material used was calculated from the total dry mass of the mixture M_d (Equation 1). Where S, L and P are the contents (%) and ρ_S, ρ_L and ρ_P are the densities of the sand, lime and PPW, respectively. The amount of PPW was calculated as a substitute for the mass of sand (Equation 2), and the amount of lime as an addition to the mass of sand plus PPW (Equation 3). V_{total} is the total volume of the sample and e is the calculated void ratio for each mixture.

$$M_d = \frac{(S+L+P)}{\left(\frac{S}{\rho_S}+\frac{L}{\rho_L}+\frac{P}{\rho_P}\right)} \cdot \frac{V_{total}}{(1+e)} \tag{1}$$

$$P = \frac{M_P}{M_S + M_P} \tag{2}$$

$$L = \frac{M_L}{M_S + M_P} \tag{3}$$

It is worth noting that the dry unit weight of each mixture decreases with the isolated increase in PPW or lime content, as can be seen in Table 3. The moisture content was defined based on Equation 4, using 5% in relation to the mass of sand (M_S) and a water/stabilizer ratio of 0.32 defined in previous tests, in order to ensure a good workability when molding. The mass of stabilizer was defined as the sum of the masses of PPW (M_P) and hydrated lime (M_L).

$$M_w = 0.05 \times M_S + 0.32 \times (M_L + M_P) \tag{4}$$

The samples were statically compacted in a tripartite cylindrical mold and in four layers of equal height. The compaction energy used in each layer was that sufficient to achieve the desired height and relative density. In this process, three samples were taken to verify the moisture content and the maximum mixing and molding time was 30 minutes. At the end of the molding process, the samples were weighed and their dimensions were measured with a precision of 0.01g and 0.01mm, respectively. Maximum tolerances of ±0.5% for moisture and ±2% for relative density were adopted. The curing process was carried out for 28 days in a humid chamber with a temperature of 23°C ± 3°C and humidity above 95%.

2.4 Undrained monotonic triaxial tests

A total of 16 monotonic triaxial tests were performed in accordance to the requirements of ASTM D4767 (ASTM, 2011). After the curing period, the samples were assembled in the triaxial cell and subjected to an upward percolation of water under low confining stress, until the volume of percolated water was greater than 2 times the volume of the sample. The saturation process was then performed by increasing the back pressure in stages of 50 kPa, keeping the effective confining stress at 10 kPa until reaching a Skempton parameter B greater than 0.95. The desired parameter B was obtained at back pressure values up to 490 kPa. Upon completion of the saturation process, the samples were isotropically consolidated under stresses of 50 kPa, 100 kPa, 200 kPa and 400 kPa. During the shear phase, the samples were subjected to triaxial compression under undrained conditions and a strain rate of 0.2 mm/min until a maximum axial strain of 20% was reached. The shearing rate was determined in previous tests in order to allow good equalization of the pore pressures. This was confirmed by checking the pore pressure on both the top and bottom of the specimen.

3. Results and discussion

A summary of the main results obtained in the monotonic triaxial tests can be seen in Table 4, where γ_d , e_i , e_c , p', q and ε_a represent the dry unit weight of molding, initial void ratio, void ratio at end of consolidation, mean effective stress, deviator stress and axial strain, respectively. Two failure modes were observed. For lower strength specimens, a tendency to bulging during shear occurred, mode A (Figure 3a). The samples of higher strength showed a well-defined shear surface, with formation of a shear band, indicating concentration of shear deformation, mode B (Figure 3b).

Figure 4 shows the stress-strain behavior and stress path under a confining stress of 50 kPa for all mixtures. Data for pure sand in the loose and medium dense state obtained by Souza Júnior et al. (2020) are also presented. The stress-strain of stabilized sand is marked by a rapid increase of the deviator stress in a small variation of the axial strain, until the peak state is reached, in which the soil failure occurs and the strength drops considerably, characterizing a brittle behavior (Figure 4a). In contrast, pure sand does not have a well-defined peak.

Table 3. Physical properties of each composition.

Code	Contents		Properties					
	PPW	Lime	$\gamma_{d_{max}}$ (kN/m³)	$\gamma_{d_{min}}$ (kN/m³)	e_{max}	e_{min}	G_s	γ_d (kN/m³)
10P3L	10%	3%	17.0	14.4	0.84	0.55	2.64	14.9
30P3L	30%	3%	17.1	12.7	1.06	0.53	2.62	13.6
10P7L	10%	7%	16.6	14.0	0.88	0.58	2.62	14.5
30P7L	30%	7%	16.0	12.1	1.15	0.62	2.60	12.9

10P3L: 10% PPW+3% Lime. 30P3L: 30% PPW+3% Lime. 10P7L: 10% PPW+7% Lime. 30P7L: 30% PPW+7% Lime

Table 4. Summary of data obtained in monotonic triaxial tests.

Mixture	Initial state				q/p'_{max}		Peak state			Critical state		Failure mode
	p' (kPa)	γ_d (kN/m³)	e_i	e_c	ε_a (%)	q/p'	ε_a (%)	p' (kPa)	q (kPa)	p' (kPa)	q (kPa)	
10P3L	50	14.91	0.768	0.762	0.41	2.22	4.24	282.17	458.20	219.36	319.80	B
	100	14.90	0.770	0.757	0.71	1.89	7.88	269.56	408.66	257.00	368.04	A
	200	14.91	0.768	0.752	1.26	1.66	6.08	340.78	522.37	265.41	375.69	B
	400	14.88	0.772	0.742	2.90	1.50	4.56	382.01	569.73	328.29	464.47	A
30P3L	50	13.56	0.928	0.923	0.46	2.68	1.73	302.96	608.84	187.96	310.90	B
	100	13.57	0.927	0.916	0.59	2.57	2.04	329.19	643.43	204.55	331.32	B
	200	13.55	0.930	0.910	0.85	2.195	1.90	416.57	796.81	216.05	348.22	B
	400	13.59	0.925	0.880	1.11	1.81	2.12	501.69	855.21	300.83	426.21	A
10P7L	50	14.49	0.810	0.804	0.36	2.65	3.88	331.04	581.27	276.28	422.88	A
	100	14.53	0.805	0.795	0.65	2.34	1.55	341.92	672.81	331.93	528.09	B
	200	14.57	0.801	0.785	0.63	2.02	3.31	379.87	639.63	325.37	499.66	A
	400	14.50	0.809	0.788	1.39	1.68	2.14	508.86	844.36	340.19	503.10	A
30P7L	50	12.88	1.021	1.015	0.53	2.89	1.74	430.07	898.97	319.45	537.68	B
	100	12.89	1.019	1.011	0.76	2.82	2.29	579.85	1189.48	377.30	620.08	B
	200	12.87	1.022	1.009	0.58	2.39	1.85	609.89	1209.09	437.89	728.37	B
	400	12.90	1.017	0.989	1.31	2.04	1.66	592.06	1164.56	408.78	679.47	B

a) b)

Figure 3. Observed failure modes for stabilized sand in triaxial tests.

A more linear stress-strain relationship is obtained up to points close to maximum ratio between q and p' (q/p'_{max}), from this point, large plastic strains appear, leading to failure and then to the critical state. Similar stress-strain behaviors were obtained in other studies that investigated the influence of stabilizers such as cement and pozzolan-lime mixtures on the mechanical behavior of soil in triaxial tests, indicating that the material investigated in this study is also a cemented soil (Amini & Hamidi, 2014; Bagheri et al., 2014; Keramatikerman et al., 2018; Li et al., 2015; Mola-Abasi et al., 2020; Rios et al., 2014; Schnaid et al., 2001; Sharma & Fahey, 2003; Vranna & Tika, 2020). Silva et al. (2023) confirmed the formation of cementitious compounds using the same mixture of PPW and lime.

Regarding the generation of pore pressure during the test, the stabilized soil shows a contractive tendency, with the emergence of a positive pore pressure peak. This phase is followed by a dilatant tendency associated with the peak strength (Figure 4b). Up to this point, the behavior is typical of dense soils. With the advancement of strains, there is a reversal of behavior and a new increase in pore pressure, culminating in a stabilization or slightly ascending trend until the end of the test. Thus, the last stage is associated with the destruction of the soil structure after the failure point (Rios et al., 2014; Sharma & Fahey, 2003; Vranna & Tika, 2020), which begins to show contractive behavior, typical of pure loose sand that liquefies.

In contrast to that observed for pure sand, a well-defined peak was obtained in the q/p' ratio at small strains for the stabilized sand (Figure 4c). The value of this parameter increases rapidly until it reaches the peak, when it then reduces to a residual plateau with a slight downward trend until the end of the test. The stress path is initially marked by a dilatant tendency until the failure point, when a significant softening occurs and the behavior is inverted to a contractive tendency, moving towards the Critical State Line (CSL) of the pure sand (Figure 4d). The contractive tendency is associated to the strain softening behavior presented by the samples in the stress-strain graph after reaching the peak.

Dilatant behaviors were observed for all stabilized sand mixtures as well as for pure sand in the medium dense state. This means that even under low relative density, the cementation caused by the incorporation of lime and PPW can change the contractive tendency of the soil to dilatant, like what occurs with the increase in densification.

In general, the stress-strain behavior of stabilized sand is similar to that of a pure dense sand until the failure point is reached, then the bonds break and the soil behaves similarly to pure sand in the loose state.

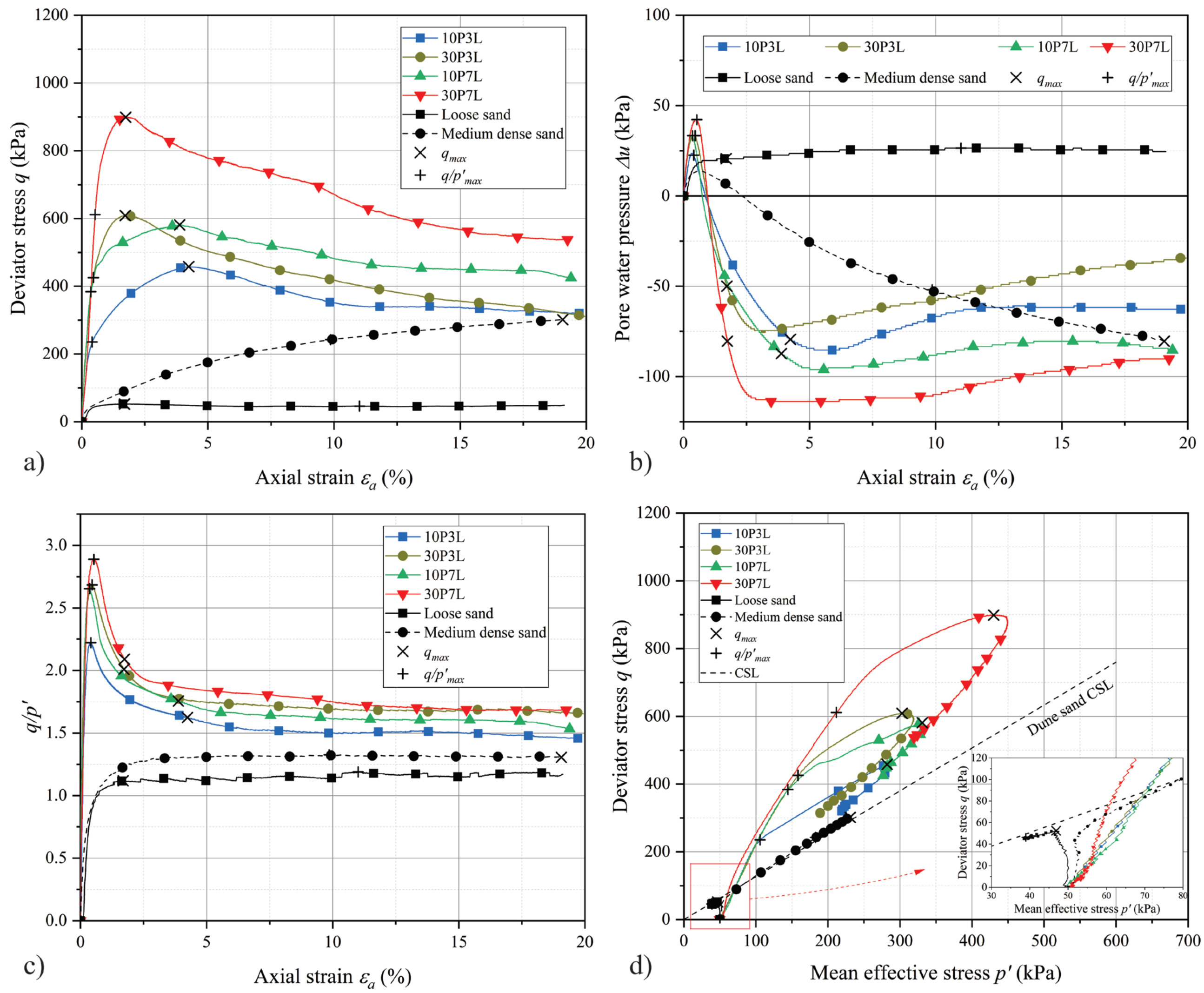

Figure 4. Effect of stabilization on dune sand response under $\sigma_3 = 50$ kPa.

3.1 Effect of the stabilizer content

The peak state is reached for average strain levels up to 2.0% for 30P3L and 30P7L mixtures, and 5.0% for 10P3L and 10P7L mixtures. This indicates that an increase in the cementation level, here assessed by peak strength, reduces strains at failure. Samples with lower stabilizer content, especially the 10P3L mixture, showed a more ductile behavior with a smaller drop in post-peak strength, a fact that according to Li et al. (2015) occurs when there is a low level of cementation between the particles.

When compared to pure sand in loose state, it is noted that stabilization is capable of increasing soil strength, with the best performance being obtained for the mixture with 30% PPW and 7% lime which achieved increments of up to 17 times. All the mixtures presented a better performance than the medium dense sand. Thus, stabilization promoted a performance gain greater than the increase in the relative density of the soil.

To better evaluate the effect of stabilizer level on sand response, the volumetric binder content parameter (B_{iv}) (Equation 5) can be used, which relates the volume of binder (PPW plus lime) to the total volume of the sample. This parameter has already been efficiently used in other studies to correlate the strength results of stabilized soil samples with the level of stabilizer (Baldovino et al., 2020; Consoli et al., 2020, 2021). In Figure 5, the parameter B_{iv} is related to the maximum deviator stress in each test.

$$B_{iv} = \frac{V_P + V_L}{V_{total}} \tag{5}$$

An increase in the volumetric binder content, by the increase in PPW and lime content separately or combined, caused a tendency to increase the q_{max}, which shows that these two components have a positive effect on the strength of the stabilized soil. However, the performances of mixtures 30P3L and 10P7L for the confining stresses of 50 kPa, 100 kPa

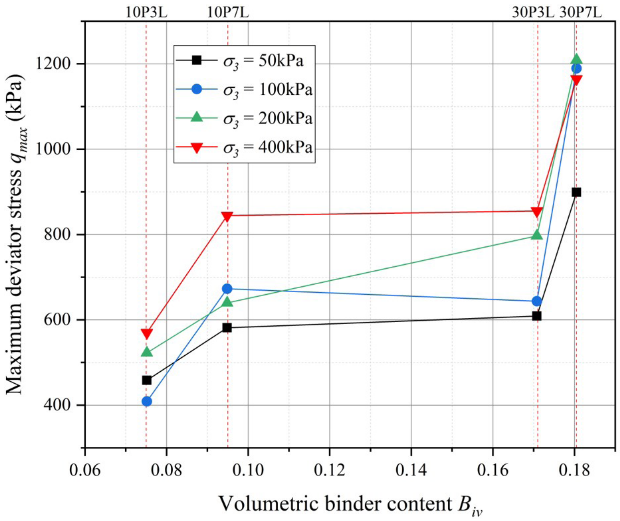

Figure 5. Influence of the volumetric binder content on the q_{max}.

and 400 kPa are similar, which generates a central plateau in the graph. This suggests that a reduction in the content of one of the stabilizer components can balance the strength gain obtained by increasing the content of the other component. An increase in the parameter B_{iv} tends to generate higher levels of cementation and consequently higher strengths. However, in a stabilizer formed by two components, the parameter B_{iv} cannot fully express the influence of each one on soil performance and is therefore not recommended for mixtures where the two contents change.

It is important to mention that the curve for the tests with 100 kPa of confining stress does not follow a trend. It is below the 50 kPa curve for sample 10P3L and above the 400 kPa curve for sample 30P7L. Some hypotheses could be the variability of the data, which was not treated in triplicate, as well as the influence of bond breakage due to the consolidation process which has a different impact on each mixture.

Compared to loose sand, stabilization reduced the contractive tendency of the soil in all mixtures. An increase in the stabilizer content, either by increasing the PPW or lime content, tends to increase the dilatant behavior of the soil. Hydration products formed in cemented soils fill the voids between grains, reducing the generation of positive excess pore pressure in undrained tests.

3.2 Effect of the confining stress

The confining stress influence on the stress-strain behavior of the stabilized sand can be seen in Figure 6, which shows the results obtained for the 30P3L mixture. There is a clear tendency for the strength to increase with the confining stress. Figure 7 shows the variation of q_{max} with the confining stress for the mixtures and the results for loose pure sand obtained by Souza Júnior et al. (2020). Between 50 kPa and 200 kPa, for example, the q_{max} value

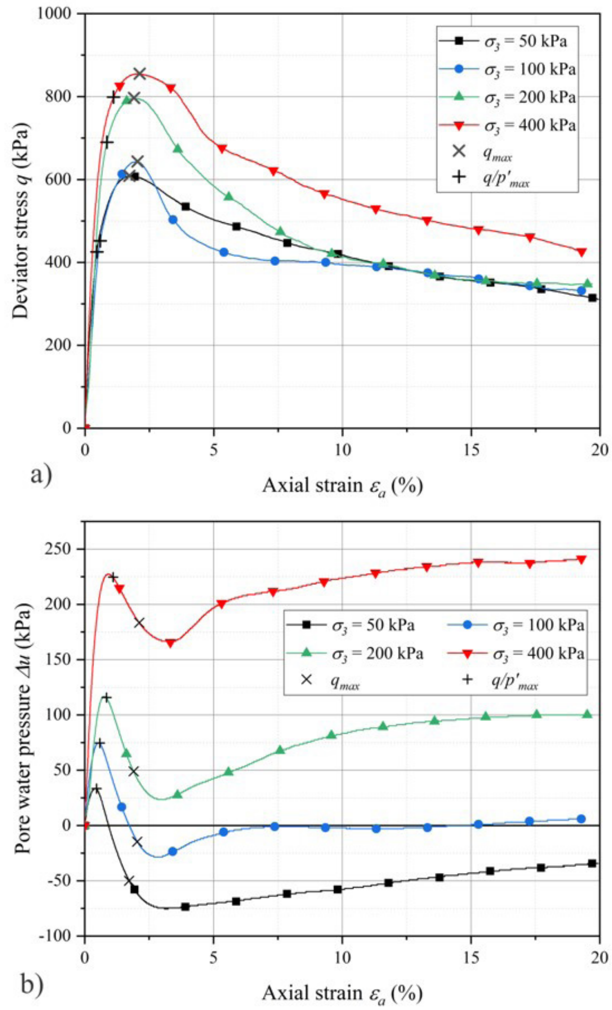

Figure 6. Confining stress effect on stabilized sand.

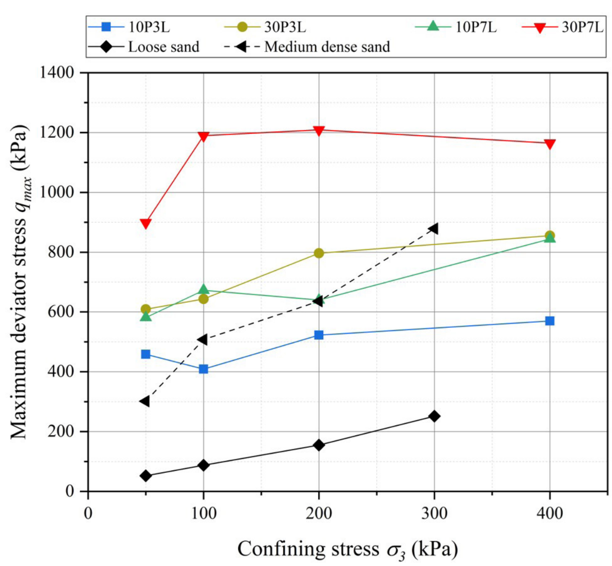

Figure 7. Variation of q_{max} with confining stress for pure and stabilized sand.

for the 30P3L mixture increased from 609 kPa to 797 kPa, representing an increase of 31%. An increasing trend was obtained by Sharma & Fahey (2003) and Bellato et al., (2020) and occurs due to an increase in the interaction between the particles which increases the internal friction resistance.

However, the behavior is not unique, in other cases there is a decrease or constancy in strength. Between 200 kPa and 400 kPa, for example, the mixture 30P7L practically maintains the same performance. This may occur due to the breaking of part of the bonds during the consolidation process, which counterbalances the gains in strength resulting from the increase in interparticle forces (Li et al., 2015; Mola-Abasi et al., 2020; Sharma & Fahey, 2003; Vranna & Tika, 2020).

This can be corroborated by Figure 8 which shows the variation of the void ratio at consolidation with the confining stress for each mixture. For the tests with 400 kPa occurs the largest variation in the void ratio for most mixtures, which may cause greater breakage of the bonds. This also suggests that 200 kPa is the yield stress of these materials. The effect of the confining stress is greater in the case of pure sand, represented by a steeper curve, which indicates greater strength gains with increasing confining stress.

An increase in the confining stress caused a reduction in the dilatant tendency. This can be attributed to a break in part of the bonds between the particles during the consolidation phase, making the response approach that of an uncemented sand in the loose state.

3.3 Liquefaction potential

The liquefaction potential (LP) of soils can be evaluated by relating the initial confining stress (σ'_{3i}) with the effective confining stress in the critical state (σ'_{3f}) through an index represented by Equation 6 (Hussain & Sachan, 2019). While positive values indicate a contractive tendency of the sample, negative values are obtained for samples with dilatant behavior where the final confining stress was higher than the initial one. The variation of LP with the initial confining stress for stabilized and pure sand is shown in Figure 9.

$$LP = \frac{\sigma'_{3i} - \sigma'_{3f}}{\sigma'_{3f}} \tag{6}$$

The pure sand in loose state showed positive values of LP, with a peak obtained for the test of 100 kPa, however there is no clear relation to the confining stress. For the medium dense sand, the values became negative, indicating a reduction in the liquefaction potential.

The stabilized sand samples showed increasing LP values with confining stress, with negative values up to σ'_{3i} equal to 200 kPa for all the mixtures. This shows that the treatment is efficient in reducing the liquefaction potential especially at low confining stresses. For σ'_{3i} equal to 400 kPa, only the 30P7L mixture presented a negative LP value.

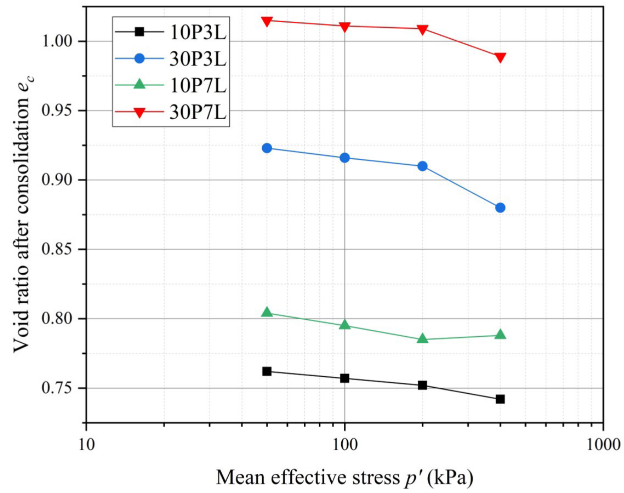

Figure 8. Variation of the void ratio after consolidation with confining stress.

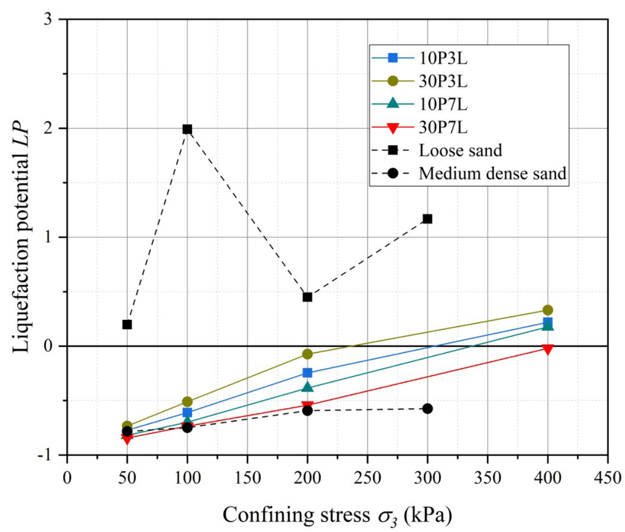

Figure 9. Variation of the liquefaction potential for pure and stabilized sand.

Thus, it can be inferred that an increase in the confining stress has a negative effect, corroborating the hypothesis that the consolidation process affected the soil structure.

Observing the curves of the mixtures 10P3L, 30P3L and 30P7L, there is a tendency of reduction of the liquefaction potential with an increase in the addition contents, however, the 30P3L mixture presented the highest LP value among the mixtures. This may be related to a non-linear influence of the fines on the liquefaction resistance of the soil, since at low lime contents and high amounts of PPW, part of the waste particles may not react chemically, working only with a physical effect. The incorporation of non-plastic fines at certain levels can reduce the liquefaction resistance of the soil for samples produced under the same relative density (Zhu et al., 2022).

3.4 Failure envelope and strength parameters

Figure 10 shows the Mohr-Coulomb peak strength envelopes for all the mixtures. The stabilized sand envelopes are positioned above the pure soil envelopes. The strength gain is attributed to an increase in the friction angle above 33.0°, higher than that found for pure sand in the medium dense state, approximately 30.5°, as well as to the emergence of a considerable cohesion intercept, of up to 108.12 kPa in the 30P3L mixture, resulting from the bonds formed between the particles (Table 5). With an increase in the cementing agent content between the 10P3L, 10P7L and 30P3L mixtures, an increase in the cohesion intercept occurred while the friction angle remained practically unchanged. However, for the 30P7L mixture there was a reduction in the cohesion intercept and increase in the friction angle. This may have been caused by variability in the performance of one of the four samples that affects the adjustment of the strength curve.

As reported by Mohamedzein & Al-Rawas (2011), cementation tends to produce small changes in the friction angle of the soil and the emergence of a cohesion intercept, which increases with cement content. Furthermore, cementation induces cohesion especially by creating bonds between particles. The friction angle can be altered by the incrustations of the cementing agent that change the shape of the soil particles. Bagheri et al. (2014) found an increase in both cohesion and peak friction angle with increasing stabilizer content for soil samples with cement, lime and rice husk ash at 28 days of curing. In any case, the tendency is usually maintained with the increase in binder content, in contrast to that presented by the 30P7L mixture.

For the mixtures with 3% lime, an increase in the PPW content tends to increase the cohesion intercept. The same happens for an increase in lime content for mixtures with 10% PPW. Thus, it can be inferred that an increase in the content of any of the additions has a beneficial effect on the strength parameters.

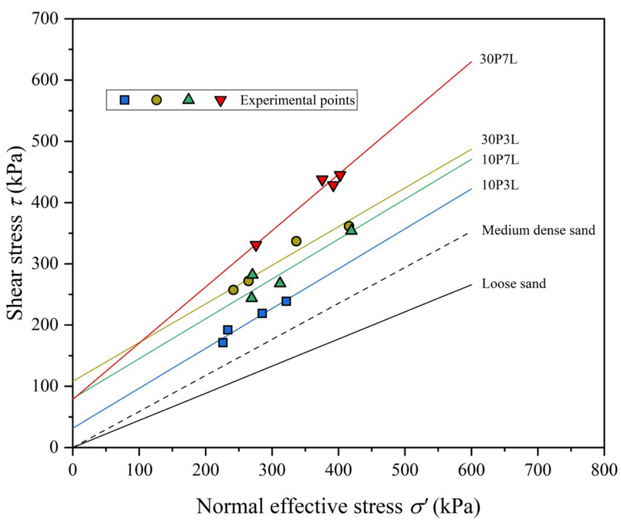

Figure 10. Peak strength envelopes of pure and stabilized sand.

Table 5. Peak strength parameters of pure and stabilized sand.

Material	Strength parameters	
	ϕ' °	c' (kPa)
Loose sand	23.89	0
Medium dense sand	30.46	0
10P3L	33.07	31.58
30P3L	32.28	108.12
10P7L	33.06	79.97
30P7L	42.59	78.44

3.5 Critical state lines

As recognized by other authors (Porcino & Marcianò, 2017; Schnaid et al., 2001; Vranna & Tika, 2020) the determination of the true critical state in cemented soil samples faces some experimental difficulties, especially due to the concentration of strains that are observed in the triaxial tests. The existence of a shear strain concentration plane and changes in the contact area between the two parts of the specimen make it difficult to stabilize the stresses. In this study, the residual test conditions were considered for the construction of the CSL both in the $p':q$ and $p':e$ planes. In Figure 11, the CSL obtained for the stabilized sand are presented, as well as the CSL referring to the pure sand obtained by Souza Júnior et al. (2020) in the $p':q$ plane.

All the stabilized sand curves are positioned above the pure sand curve, with a tendency to increase the slope with the B_{iv} parameter, although the curves for the 10P7L and 30P3L mixtures are very close. According to Vranna & Tika (2020), in the critical state, the structure of the cemented soil present in the shear band is formed by fragments of the cementing agent that were formed with the failure process,

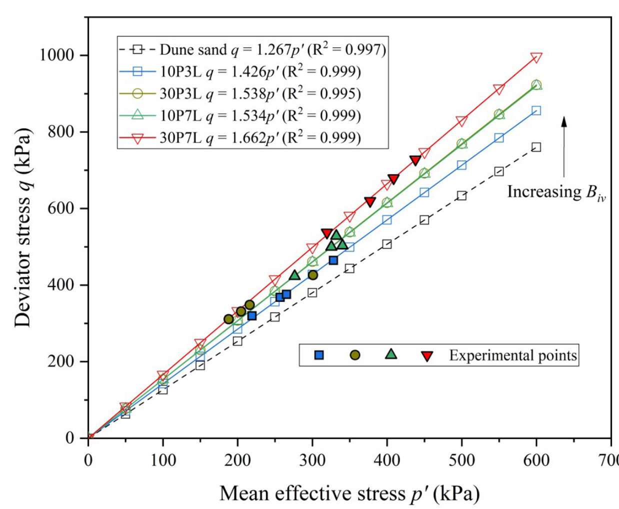

Figure 11. Critical state lines of pure and stabilized sand in the $p':q$ plane.

as well as more granular particles with incrustations and different shapes from those existing in the pure sand. Thus, an increase in the cementation level tends to generate a structure with superior frictional strength, which explains an increase in the friction angle in the critical state.

According to Rios et al. (2014), the behavior of cemented soil is governed by the performance of the cementing agent, and subsequently by the fragments formed after failure. These researchers also found the CSL for cemented soil to be steeper than for pure soil. For Ajorloo et al. (2012), an increase in particle roughness, due to the covering by the cementing agent or bonds that remained even after failure, may contribute to the increase in the slope of the CSL. Furthermore, this effect is similar to that obtained with the incorporation of non-plastic fines in the CSL of uncemented sands (Zhu et al., 2022).

In the $p' : e$ plane, the equation presented by Schofield & Wroth (1968) was used to define the CSL for each composition. The final states reached for each confining stress were plotted together with the CSL obtained, to visualize the fit degree (Figure 12). The data referring to the 400 kPa test for the 30P7L mixture was not used, as it is too far from what was obtained in the other confining stresses. As in the $p' : q$ plane, the stabilized sand curves remained above the pure sand curve and are higher the greater the stabilizer content.

The critical state parameters M, ϕ_{cs}, Γ and λ that were obtained in the line fits in Figures 11 and 12 are presented in Table 6. The increase in the value of M and ϕ_{cs} with sand

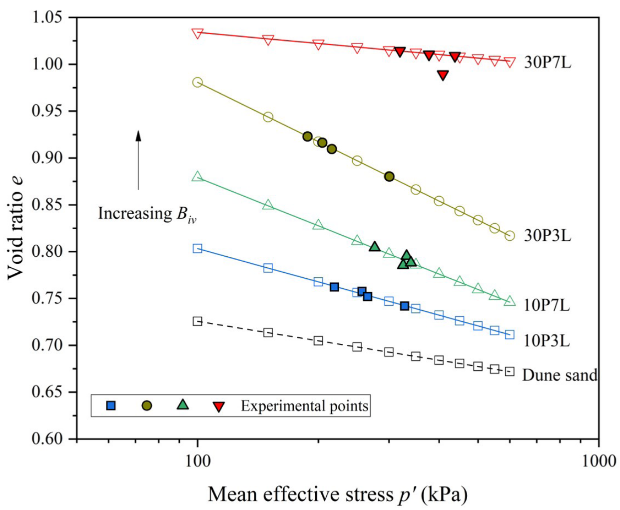

Figure 12. Critical state lines of pure and stabilized sand in the $p' : e$ plane.

Table 6. Critical state parameters of pure and stabilized sand.

Material	M	ϕ_{CS} °	Γ	λ
Dune sand	1.267	31.50	0.726	0.03
10P3L	1.426	35.17	0.803	0.05
30P3L	1.538	37.74	0.981	0.09
10P7L	1.534	37.64	0.871	0.02
30P7L	1.654	40.41	1.028	0.01

stabilization is in agreement with other research on cement-stabilized soils (Schnaid et al., 2001; Vranna & Tika, 2020).

4. Conclusion

In this research, the influence of the incorporation of porcelain polishing waste and hydrated lime on the undrained response of a dune sand was evaluated by means of monotonic triaxial tests. The confining stress, lime content and PPW content variables were combined and the response was evaluated through the stress-strain behavior, stress path and soil strength envelopes.

The stress-strain behavior of stabilized sand is marked by a brittle response and dilatant trend until the material failure, when its destructuring causes a reversion to a contractive trend similar to that presented by pure loose sand. An increase in the confining stress causes an increase in soil performance and a reduction in the dilatant behavior, resulting from the breakage of part of the bonds formed due to the consolidation process.

Compared to pure sand, there was a gain in strength up to 17 times, with an increase in the friction angle, higher than that of medium dense sand, and the emergence of a cohesion intercept up to 108.1 kPa, resulting from the cementation between the particles. Although there is a tendency for strength to increase with the B_{iv} parameter, it has not proved suitable for assessing situations where the contents of the two components have varied in different directions.

Stabilization reduced the liquefaction potential of the soil, but the effect of each addition on this parameter needs to be further studied. The presence of unreacted fines may also influence the undrained behavior of the soil. Furthermore, the confining stress has a negative effect on the liquefaction resistance of the stabilized soil. Finally, a superior frictional strength in the critical state was obtained with an increase in the cementation level.

Acknowledgements

The authors acknowledge the company Ceramics Elizabeth for supplying the porcelain polishing waste used in this study. The authors also thank the Higher Education Personnel Improvement Coordination (CAPES) and the National Council for Scientific and Technological Development (CNPQ) for the financial support granted for this study.

Declaration of interest

The authors have no conflicts of interest to declare. All co-authors have observed and affirmed the contents of the paper and there is no financial interest to report.

Authors' contributions

José Daniel Jales Silva: conceptualization, data curation, methodology, formal analysis, investigation, writing – original

draft, writing – review & editing. Olavo Francisco dos Santos Júnior: conceptualization, project administration, supervision, funding acquisition, writing – review & editing. Osvaldo de Freitas Neto: conceptualization, supervision, formal analysis, writing – review & editing. Romário Stéffano Amaro da Silva: conceptualization, methodology, writing – review & editing. Manoel Leandro Araújo e Farias: conceptualization, methodology, writing – review & editing. Bruna Silveira Lira: conceptualization, writing – review & editing.

Data availability

The datasets generated analyzed in the course of the current study are available from the corresponding author upon request.

Declaration of use of generative artificial intelligence

This work was prepared without the assistance of any generative artificial intelligence.

List of symbols and abbreviations

c'	Cohesion intercept
d_{10}	Effective diameter
d_{50}	Mean diameter
e	Void ratio
e_c	Void ratio at end of consolidation
e_i	Initial void ratio
e_{max}	Maximum void ratio
e_{min}	Minimum void ratio
p'	Mean effective stress
q	Deviator stress
q/p'_{max}	Maximum ratio between q and p'
q_{max}	Maximum deviator stress
B	Pore water pressure coefficient
B_{iv}	Volumetric binder content
C_c	Coefficient of curvature
CSL	Critical state line
C_u	Coefficient of uniformity
G_s	Specific gravity
L	Lime content
LP	Liquefaction potential
M	Slope of CSL in $p':q$ space
M_d	Total dry mass of the mixture
M_L	Mass of lime particles
ML	Low plasticity silt
M_S	Mass of sand particles
M_P	Mass of PPW particles
M_w	Mass of water
P	PPW content
PPW	Porcelain polishing waste
R^2	Coefficient of determination
S	Sand content
SP	Poorly graded sand
V_{total}	Total volume of the sample
γ_d	Dry unit weight
Δu	Excess pore water pressure
ε_a	Axial strain
λ	Slope of CSL in $e:\log p'$ space
ρ_S	Density of sand particles
ρ_L	Density of lime particles
ρ_P	Density of PPW particles
ρ_w	Density of water
σ'	Normal effective stress
σ_3	Confining stress
σ'_{3i}	Initial effective confining stress
σ'_{3f}	Final effective confining stress
τ	Shear stress
ϕ'	Internal friction angle
Γ	Intercept of CSL in $e:\log p'$ space

References

Abbasi, N., & Mahdieh, M. (2018). Improvement of geotechnical properties of silty sand soils using natural pozzolan and lime. *International Journal of Geo-Engineering*, 9(1), 4. http://doi.org/10.1186/s40703-018-0072-4.

Ajorloo, A.M., Mroueh, H., & Lancelot, L. (2012). Experimental investigation of cement treated sand behavior under triaxial test. *Geotechnical and Geological Engineering*, 30(1), 129-143. http://doi.org/10.1007/s10706-011-9455-4.

Amini, Y., & Hamidi, A. (2014). Triaxial shear behavior of a cement-treated sand–gravel mixture. *Journal of Rock Mechanics and Geotechnical Engineering*, 6(5), 455-465. http://doi.org/10.1016/j.jrmge.2014.07.006.

ASTM D4767. (2011). *Standard Test Method for Consolidated Undrained Triaxial Compression Test for Cohesive Soils*. ASTM International, West Conshohocken, PA, USA. https://10.1520/D4767-11R20.

Bagheri, Y., Ahmad, F., & Ismail, M.A.M. (2014). Strength and mechanical behavior of soil–cement–lime–rice husk ash (soil–CLR) mixture. *Materials and Structures*, 47(1-2), 55-66. http://doi.org/10.1617/s11527-013-0044-2.

Baldovino, J.J.A., Izzo, R.L.S., Silva, É.R., & Lundgren Rose, J. (2020). Sustainable use of recycled-glass powder in soil stabilization. *Journal of Materials in Civil Engineering*, 32(5), 04020080. http://doi.org/10.1061/(ASCE)MT.1943-5533.0003081.

Bellato, D., Spagnoli, G., & Simonini, P. (2020). Mineralogical and mechanical analysis of cement-stabilised sands. *Proceedings of the Institution of Civil Engineers - Ground Improvement*, 173(1), 51-60. http://doi.org/10.1680/jgrim.18.00059.

Castro, G., & Poulos, S.J. (1977). Factors affecting liquefaction and cyclic mobility. *Journal of the Geotechnical Engineering*

Division, 103(6), 501-516. http://doi.org/10.1061/AJGEB6.0000433.

Consoli, N.C., Bittar Marin, E.J., Quiñónez Samaniego, R.A., Heineck, K.S., & Johann, A.D.R. (2019a). Use of sustainable binders in soil stabilization. *Journal of Materials in Civil Engineering*, 31(2), 06018023. http://doi.org/10.1061/(ASCE)MT.1943-5533.0002571.

Consoli, N.C., Carretta, M.S., Leon, H.B., Schneider, M.E.B., Reginato, N.C., & Carraro, J.A.H. (2020). Behaviour of cement-stabilised silty sands subjected to harsh environmental conditions. *Proceedings of the Institution of Civil Engineers - Geotechnical Engineering*, 173(1), 40-48. http://doi.org/10.1680/jgeen.18.00243.

Consoli, N.C., Leon, H.B., Silva Carretta, M., Daronco, J.V.L., & Lourenço, D.E. (2019b). The effects of curing time and temperature on stiffness, strength and durability of sand-environment friendly binder blends. *Soil and Foundation*, 59(5), 1428-1439. http://doi.org/10.1016/j.sandf.2019.06.007.

Consoli, N.C., Silva Carretta, M., Festugato, L., Leon, H.B., Tomasi, L.F., & Heineck, K.S. (2021). Ground waste glass–carbide lime as a sustainable binder stabilising three different silica sands. *Geotechnique*, 71(6), 480-493. http://doi.org/10.1680/jgeot.18.P.099.

Fergany, E., & Omar, K. (2017). Liquefaction potential of Nile delta, Egypt. *NRIAG Journal of Astronomy and Geophysics*, 6(1), 60-67. http://doi.org/10.1016/j.nrjag.2017.01.004.

Gautam, D., Magistris, F.S., & Fabbrocino, G. (2017). Soil liquefaction in Kathmandu valley due to 25 April 2015 Gorkha, Nepal earthquake. *Soil Dynamics and Earthquake Engineering*, 97, 37-47. http://doi.org/10.1016/j.soildyn.2017.03.001.

Ghadr, S., & Assadi-Langroudi, A. (2019). Effect of grain size and shape on undrained behaviour of sands. *International Journal of Geosynthetics and Ground Engineering*, 5(3), 18. http://doi.org/10.1007/s40891-019-0170-1.

Ghorbani, A., Salimzadehshooiili, M., Medzvieckas, J., & Kliukas, R. (2018). Strength characteristics of cement-rice husk ash stabilised sand-clay mixture reinforced with polypropylene fibers. *The Baltic Journal of Road and Bridge Engineering*, 13(4), 447-474. http://doi.org/10.7250/bjrbe.2018-13.428.

Horpibulsuk, S., Rachan, R., & Raksachon, Y. (2009). Role of fly ash on strength and microstructure development in blended cement stabilized silty clay. *Soil and Foundation*, 49(1), 85-98. http://doi.org/10.3208/sandf.49.85.

Hussain, M., & Sachan, A. (2019). Dynamic characteristics of natural kutch sandy soils. *Soil Dynamics and Earthquake Engineering*, 125, 105717. http://doi.org/10.1016/j.soildyn.2019.105717.

Ishihara, K., Tatsuoka, F., & Yasuda, S. (1975). Undrained deformation and liquefaction of sand under cyclic stresses. *Soil and Foundation*, 15(1), 29-44. http://doi.org/10.3208/sandf1972.15.29.

Jacoby, P.C., & Pelisser, F. (2015). Pozzolanic effect of porcelain polishing residue in Portland cement. *Journal of Cleaner Production*, 100, 84-88. http://doi.org/10.1016/j.jclepro.2015.03.096.

Keramatikerman, M., Chegenizadeh, A., & Nikraz, H. (2017). Experimental study on effect of fly ash on liquefaction resistance of sand. *Soil Dynamics and Earthquake Engineering*, 93, 1-6. http://doi.org/10.1016/j.soildyn.2016.11.012.

Keramatikerman, M., Chegenizadeh, A., Yilmaz, Y., & Nikraz, H. (2018). Effect of lime treatment on static liquefaction behavior of sand–bentonite mixtures. *Journal of Materials in Civil Engineering*, 30(11), 06018017. http://doi.org/10.1061/(ASCE)MT.1943-5533.0002500.

Kolay, P.K., Puri, V.K., Lama Tamang, R., Regmi, G., & Kumar, S. (2019). Effects of fly ash on liquefaction characteristics of Ottawa sand. *International Journal of Geosynthetics and Ground Engineering*, 5(2), 6. http://doi.org/10.1007/s40891-019-0158-x.

Krishnan, J., & Shukla, S. (2021). The utilisation of colloidal silica grout in soil stabilisation and liquefaction mitigation: A state of the art review. *Geotechnical and Geological Engineering*, 39(4), 2681-2706. http://doi.org/10.1007/s10706-020-01651-5.

Li, D., Liu, X., & Liu, X. (2015). Experimental study on artificial cemented sand prepared with ordinary portland cement with different contents. *Materials (Basel)*, 8(7), 3960-3974. http://doi.org/10.3390/ma8073960.

Li, L.G., Ouyang, Y., Zhuo, Z.Y., & Kwan, A.K.H. (2021). Adding ceramic polishing waste as filler to reduce paste volume and improve carbonation and water resistances of mortar. *Advances in Bridge Engineering*, 2(1), 3. http://doi.org/10.1186/s43251-020-00019-2.

Mahmoudi, Y., Cherif Taiba, A., Hazout, L., Belkhatir, M., & Baille, W. (2020). Packing density and overconsolidation ratio effects on the mechanical response of granular soils. *Geotechnical and Geological Engineering*, 38(1), 723-742. http://doi.org/10.1007/s10706-019-01061-2.

Mahvash, S., López-Querol, S., & Bahadori-Jahromi, A. (2018). Effect of fly ash on the bearing capacity of stabilised fine sand. *Proceedings of the Institution of Civil Engineers -. Ground Improvement*, 171(2), 82-95. http://doi.org/10.1680/jgrim.17.00036.

Matos, P.R., Jiao, D., Roberti, F., Pelisser, F., & Gleize, P.J.P. (2020). Rheological and hydration behaviour of cement pastes containing porcelain polishing residue and different water-reducing admixtures. *Construction & Building Materials*, 262, 120850. http://doi.org/10.1016/j.conbuildmat.2020.120850.

Matos, P.R., Oliveira, A.L., Pelisser, F., & Prudêncio Júnior, L.R. (2018a). Rheological behavior of Portland cement pastes and self-compacting concretes containing porcelain polishing residue. *Construction & Building Materials*, 175, 508-518. http://doi.org/10.1016/j.conbuildmat.2018.04.212.

Matos, P.R., Prudêncio Junior, L.R., Oliveira, A.L., Pelisser, F., & Gleize, P.J.P. (2018b). Use of porcelain polishing residue as a supplementary cimentitious material in self-compacting concrete. *Construction & Building Materials*, 193, 623-630. http://doi.org/10.1016/j.conbuildmat.2018.10.228.

Medeiros, A.G., Gurgel, M.T., Silva, W.G., Oliveira, M.P., Ferreira, R.L.S., & Lima, F.J.N. (2021). Evaluation of the mechanical and durability properties of eco-efficient concretes produced with porcelain polishing and scheelite wastes. *Construction & Building Materials*, 296, 123719. http://doi.org/10.1016/j.conbuildmat.2021.123719.

Minyong, L., Gomez, G.M., Maya, E.K., & Katerina, Z. (2022). Effect of light biocementation on the liquefaction triggering and post-triggering behavior of loose sands. *Journal of Geotechnical and Geoenvironmental Engineering*, 148(1), 04021170. http://doi.org/10.1061/(ASCE)GT.1943-5606.0002707.

Mohamedzein, Y.E.A., & Al-Rawas, A.A. (2011). Cement-stabilization of Sabkha soils from Al-Auzayba, Sultanate of Oman. *Geotechnical and Geological Engineering*, 29(6), 999-1008. http://doi.org/10.1007/s10706-011-9432-y.

Mola-Abasi, H., Saberian, M., Semsani, S.N., Li, J., & Khajeh, A. (2020). Triaxial behaviour of zeolite-cemented sand. *Proceedings of the Institution of Civil Engineers -. Ground Improvement*, 173(2), 82-92. http://doi.org/10.1680/jgrim.18.00009.

Ni, X.Q., Zhang, Z., Ye, B., & Zhang, S. (2022). Unique relation between pore water pressure generated at the first loading cycle and liquefaction resistance. *Engineering Geology*, 296, 106476. http://doi.org/10.1016/j.enggeo.2021.106476.

Porcino, D.D., & Marcianò, V. (2017). Bonding degradation and stress–dilatancy response of weakly cemented sands. *Geomechanics and Geoengineering*, 12(4), 221-233. http://doi.org/10.1080/17486025.2017.1347287.

Rios, S., Viana da Fonseca, A., & Baudet, B.A. (2014). On the shearing behaviour of an artificially cemented soil. *Acta Geotechnica*, 9(2), 215-226. http://doi.org/10.1007/s11440-013-0242-7.

Riveros, G.A., & Sadrekarimi, A. (2020). Liquefaction resistance of Fraser River sand improved by a microbially-induced cementation. *Soil Dynamics and Earthquake Engineering*, 131, 106034. http://doi.org/10.1016/j.soildyn.2020.106034.

Rogers, C.D.F., Glendinning, S.T., & Roff, T.E.J. (1997). Lime modification of clay soils for construction expediency. *Proceedings of the Institution of Civil Engineers - Geotechnical Engineering*, 125(4), 242-249. http://doi.org/10.1680/igeng.1997.29660.

Sana, H., & Nath, S.K. (2016). Liquefaction potential analysis of the Kashmir valley alluvium, NW Himalaya. *Soil Dynamics and Earthquake Engineering*, 85, 11-18. http://doi.org/10.1016/j.soildyn.2016.03.009.

Schnaid, F., Prietto, P.D.M., & Consoli, N.C. (2001). Characterization of cemented sand in triaxial compression. *Journal of Geotechnical and Geoenvironmental Engineering*, 127(10), 857-868. http://doi.org/10.1061/(ASCE)1090-0241(2001)127:10(857).

Schofield, A., & Wroth, C.P. (1968). *Critical state soil mechanics*. McGraw-Hill.

Sharma, M., Satyam, N., & Reddy, K.R. (2021). State of the art review of emerging and biogeotechnical methods for liquefaction mitigation in sands. *Journal of Hazardous, Toxic and Radioactive Waste*, 25(1), 03120002. http://doi.org/10.1061/(ASCE)HZ.2153-5515.0000557.

Sharma, S.S., & Fahey, M. (2003). Evaluation of cyclic shear strength of two cemented calcareous soils. *Journal of Geotechnical and Geoenvironmental Engineering*, 129(7), 608-618. http://doi.org/10.1061/(ASCE)1090-0241(2003)129:7(608).

Silva, J.D.J., Santos Júnior, O.F., & Paiva, W. (2023). Compressive and tensile strength of aeolian sand stabilized with porcelain polishing waste and hydrated lime. *Soils and Rocks*, 46(1), e2023002322. http://doi.org/10.28927/SR.2023.002322.

Simatupang, M., Mangalla, L.K., Edwin, R.S., Putra, A.A., Azikin, M.T., Aswad, N.H., & Mustika, W. (2020). The mechanical properties of fly-ash-stabilized sands. *Geosciences*, 10(4), 132. http://doi.org/10.3390/geosciences10040132.

Smitha, S., & Rangaswamy, K. (2021). The potential use of biopolymers as a sustainable alternative for liquefaction mitigation - a review. In R.M. Singh, K.P. Sudheer & B. Kurian (Eds.), *Advances in Civil Engineering. Lecture Notes in Civil Engineering* (Vol. 83, pp. 25-34). Springer. http://dx.doi.org/10.1007/978-981-15-5644-9_3.

Sousa, I.V., Jaramillo Nieves, L.J., Dal-Bó, A.G., & Bernardin, A.M. (2022). Valorization of porcelain tile polishing residue in the production of cellular ceramics. *Cleaner Engineering and Technology*, 6, 100381. http://doi.org/10.1016/j.clet.2021.100381.

Souza Júnior, P.L., Santos Júnior, O.F., & Fontoura, T.B. (2020). Drained and undrained behavior of an aeolian sand from Natal, Brazil. *Soils and Rocks*, 43(2), 263-270. http://doi.org/10.28927/SR.432263.

Sze, H.Y., & Yang, J. (2014). Failure modes of sand in undrained cyclic loading: impact of sample preparation. *Journal of Geotechnical and Geoenvironmental Engineering*, 140(1), 152-169. http://doi.org/10.1061/(ASCE)GT.1943-5606.0000971.

Triantafyllos, P.K., Georgiannou, V.N., Dafalias, Y.F., & Georgopoulos, I.O. (2020). New findings on the evolution of the instability surface of loose sand. *Acta Geotechnica*, 15(1), 197-221. http://doi.org/10.1007/s11440-019-00887-7.

Vranna, A., & Tika, T. (2020). Undrained monotonic and cyclic response of weakly cemented sand. *Journal of Geotechnical and Geoenvironmental Engineering*, 146(5), 04020018. http://doi.org/10.1061/(ASCE)GT.1943-5606.0002246.

Wang, Q., Wang, L., Zhong, X., Guo, P., Wang, J., Ma, H., Gao, Z., & Wang, H. (2021). Dynamic behaviour and constitutive relationship of saturated fly ash-modified loess. *European Journal of Environmental and Civil Engineering*, 25(7), 1302-1317. http://doi.org/10.1080/19648189.2019.1577181.

Xiao, P., Liu, H., Stuedlein, A.W., Evans, T.M., & Xiao, Y. (2019). Effect of relative density and biocementation on cyclic response of calcareous sand. *Canadian Geotechnical Journal*, 56(12), 1849-1862. http://doi.org/10.1139/cgj-2018-0573.

Yang, J., Liang, L.B., & Chen, Y. (2022). Instability and liquefaction flow slide of granular soils: the role of initial shear stress. *Acta Geotechnica*, 17(1), 65-79. http://doi.org/10.1007/s11440-021-01200-1.

Zhang, X., & Russell, A.R. (2021). Liquefaction potential and effective stress of fiber-reinforced sand during undrained cyclic loading. *Journal of Geotechnical and Geoenvironmental Engineering*, 147(7), 04021042. http://doi.org/10.1061/(ASCE)GT.1943-5606.0002530.

Zhao, M., Liu, G., Zhang, C., Guo, W., & Luo, Q. (2019). State-of-the-art of colloidal silica-based soil liquefaction mitigation: an emerging technique for ground improvement. *Applied Sciences (Basel, Switzerland)*, 10(1), 15. http://doi.org/10.3390/app10010015.

Zhu, Z., Dupla, J.C., Canou, J., & Foerster, E. (2022). Experimental study of liquefaction resistance: effect of non-plastic silt content on sand matrix. *European Journal of Environmental and Civil Engineering*, 26(7), 2671-2689. http://doi.org/10.1080/19648189.2020.1765198.

Zhu, Z., Zhang, F., Peng, Q., Dupla, J.C., Canou, J., Cumunel, G., & Foerster, E. (2021). Effect of the loading frequency on the sand liquefaction behaviour in cyclic triaxial tests. *Soil Dynamics and Earthquake Engineering*, 147, 106779. http://doi.org/10.1016/j.soildyn.2021.106779.